regenerated epithelium showed squamous metaplasia. Transmission electron microscopy also showed squamous changes in the superficial cell layer of the regenerated epithelium. The most common pathogenic setting for squamous metaplasia is chronic cystitis [26]. Because in the present study the demucosalized gastric flap grafted with urothelial cell sheets was in the abdominal cavity, exposure of its surface to ascites may induce inflammation that resulted in the squamous change.

Li *et al.* [27] reported gastrointestinal mesenchyme/stroma-urothelium interactions; they performed tissue recombination experiments with combinations of rectal mesenchyme and urothelium from embryonic, newborn and adult samples. The tissue recombinants were grafted beneath the kidney capsule of adult male athymic nude mice. The urothelium had the plasticity to change into an intestinal-like epithelium as a result of mesenchymal/stromal stimulation from the gastrointestinal tract. However, they also reported that gastric stromal layers did not induce the transdifferentiation of urothelium [28]; similarly, there was no such transdifferentiation in the present study.

Of the eight urothelial cell sheets autografted in dogs five had viable regenerated epithelium, but three did not. All three demucosalized flaps where urothelial cell sheets were unable to attach had severe surface haematoma. Apparently it is important for cell-sheet attachment to control bleeding from the demucosalized surfaces. The stability of the autografted urothelial cell sheets with no fixation was incomplete in these cases. Additionally, as xenogenic 3T3 feeder cells were used as a feeder layer for *in vitro* culture, an immunologically mediated reaction cannot be excluded [29]. Schaefer *et al.* [4] noted that epithelialization of their demucosalized gastrointestinal surfaces with urothelial cells grown in co-culture with 3T3 feeder cells was more efficient than with urothelial cells grown in monoculture, although they used collagen membranes.

The flaps had shrunk and the smooth muscle was atrophied at death. Both would be caused by lack of stretch, as in the present model there was no augmentation cystoplasty. Currently we are using augmentation cystoplasty with demucosalized intestinal segments covered with cultured urothelial cell sheets.

In conclusion, we confirm that cultured urothelial cell sheets obtained using temperature-responsive culture dishes readily transplant onto demucosalized gastric flaps to produce multilayered epithelium with no glandular epithelial cells *in vivo*. This versatile method should prove useful in urinary tract tissue engineering and surgical reconstruction.

ACKNOWLEDGEMENTS

Dr Kuniko Tsunoyama, Ayako Nishimoto, Shuichi Sekine and Chie Takahashi assisted with surgical procedures. Shigeru Horita, Mayuko Kawashima and Hideki Nakayama provided assistance and advice with electron microscopy interpretation. Dr T.T. Sun (New York University, NY) kindly provided rabbit antiserum to total bovine uroplakins. Prof David W. Grainger (Colorado State University, Ft. Collins, CO USA) provided useful technical comments and editing. The present work was supported by the Japan Society for the Promotion of Science, Grant-in-Aid for Scientific Research (14571524, 13558119) and The Promotion and Mutual Aid Corporation for Private School of Japan.

CONFLICT OF INTEREST

None declared. Source of funding: Japan Society for the Promotion of Science, Grant-in-Aid for Scientific Research (14571524, 13558119).

REFERENCES

Gerharz EW, Turner WH, Kalble T, Woodhouse CR. Metabolic and functional consequences of urinary reconstruction with bowel. *BJU Int* 2003; **91**: 143–9

Mills RD, Studer UE. Metabolic consequences of continent urinary diversion. *J Urol* 1999; **161**: 1057–66

Merguerian P, Chavez DR, Hakim S. Grafting of cultured uroepithelium and bladder mucosa into de-epithelialized segments of colon in rabbits. *J Urol* 1994; **152**: 671–4

Schaefer BM, Lorenz C, Back W *et al.* Autologous transplantation of urothelium into demucosalized gastrointestinal segments: evidence for epithelialization and differentiation of *in vitro* expanded and transplanted urothelial cells. *J Urol* 1998; **159**: 284–90

Aktug T, Ozdemir T, Agartan C, Ozer E, Olguner M, Akgur FM. Experimentally prefabricated bladder. *J Urol* 2001; **165**: 2055–8

Shiroyanagi Y, Yamato M, Yamazaki Y, Toma H, Okano T. Transplantable urothelial cell sheets harvested noninvasively from temperature-responsive culture surfaces by reducing temperature. *Tissue Eng* 2003; **9**: 1005–12

Kushida A, Yamato M, Kikuchi A, Okano T. Two-dimensional manipulation of differentiated Madin-Darby canine kidney (MDCK) cell sheets: the noninvasive harvest from temperature-responsive culture dishes and transfer to other surfaces. *J Biomed Mater Res* 2001; **54**: 37–46

Yamato M, Utsumi M, Kushida A, Konno C, Kikuchi A, Okano T. Thermo-responsive culture dishes allow the intact harvest of multilayered keratinocyte sheets without dispase by reducing temperature. *Tissue Eng* 2001; **7**: 473–80

Hirose M, Kwon OH, Yamato M, Kikuchi A, Okano T. Creation of designed shape cell sheets that are noninvasively harvested and moved onto another surface. *Biomacromolecules* 2000; **1**: 377–81

Rheinwald JG, Green H. Serial cultivation of strains of human epidermal keratinocytes: the formation of keratinizing colonies from single cells. *Cell* 1975; **6**: 331–43

Inoue T, Osatake H. A new drying method of biological specimens for scanning electron microscopy: the t-butyl alcohol freeze-drying method. *Arch Histol Cytol* 1988; **51**: 53–9

Gonzalez R, Buson H, Reid C, Reinberg Y. Seromuscular colocystoplasty lined with urothelium: experience with 16 patients. *Urology* 1995; **45**: 124–9

Kropp BP, Rippy MK, Badylak SF *et al.* Regenerative urinary bladder augmentation using small intestinal submucosa. urodynamic and histopathologic assessment in long-term canine bladder augmentations. *J Urol* 1996; **155**: 2098–104

Probst M, Piechota HJ, Dahiya R, Tanagho EA. Homologous bladder

augmentation in dog with the bladder acellular matrix graft. *BJU Int* 2000; **85**: 362–71

Oberpenning F, Meng J, Yoo JJ, Atala A. De novo reconstitution of a functional mammalian urinary bladder by tissue engineering. *Nat Biotechnol* 1999; **17**: 149–55

Cilento BG, Freeman MR, Schneck FX, Retik AB, Atala A. Phenotypic and cytogenetic characterization of human bladder urothelia expanded *in vitro*. *J Urol* 1994; **152**: 665–70

Yamada N, Okano T, Sakai H, Karikusa F, Sawasaki Y, Sakurai Y. Thermo-responsive polymeric surfaces; control of attachment and detachment of cultured cells. *Makromol Chem Rapid Commun* 1990; **11**: 571–6

Okano T, Yamada N, Sakai H, Sakurai Y. A novel recovery system for cultured cells using plasma-treated polystyrene dishes grafted with poly (*N*-isopropylacrylamide). *J Biomed Mater Res* 1993; **27**: 1243–51

Shimizu T, Yamato M, Isoi Y *et al.* Fabrication of pulsatile cardiac tissue grafts using a novel 3-dimensional cell sheet manipulation technique and temperature-responsive cell culture surfaces. *Circ Res* 2002; **90**: 40

Yamato M, Konno C, Utsumi M, Kikuchi A, Okano T. Thermally responsive polymer-grafted surfaces facilitate patterned cell seeding and co-culture. *Biomaterials* 2002; **23**: 561–7

Kushida A, Yamato M, Konno C, Kikuchi A, Sakurai Y, Okano T. Decrease in culture temperature releases monolayer endothelial cell sheets together with deposited fibronectin matrix from temperature-responsive culture surfaces. *J Biomed Mater Res* 1999; **45**: 355–62

Wechselberger G, Russell RC, Neumeister MW, Schoeller T, Piza-Katzer H, Rainer C. Successful transplantation of three tissue-engineered cell types using capsule induction technique and fibrin glue as a delivery vehicle. *Plast Reconstr Surg* 2002; **110**: 123–9

Atala A, Vacanti JP, Peters CA, Mandell J, Retik AB, Freeman MR. Formation of urothelial structures in vivo from dissociated cells attached to biodegradable polymer scaffolds in vitro. *J Urol* 1992; **148**: 658–62

Tachibana M, Nagamatsu GR, Addonizio JC. Ureteral replacement using collagen sponge tube grafts. *J Urol* 1985; **133**: 866–9

Sun TT, Zhao H, Provet J, Aebi U, Wu XR. Formation of asymmetric unit membrane during urothelial differentiation. *Mol Biol Rep* 1996; **23**: 3–11

Eagan JWJ. Urothelial neoplasms: pathologic anatomy. In Hill GS ed. *Uropathology*, **Vol. II**. New York: Churchill Livingstone, 1989: 719–92

Li Y, Liu W, Hayward SW, Cunha GR, Baskin LS. Plasticity of the urothelial phenotype: effects of gastro-intestinal mesenchyme/stroma and implications for urinary tract reconstruction. *Differentiation* 2000; **66**: 126–35

Master VA, Wei G, Liu W, Cunha GS, Baskin LS. Abstract of Section on Urology, American Academy of Pediatrics. National Conference and Exhibition. Boston, MA, USA 2002: 108–9

Cairns BA, deSerres S, Brady LA, Hultman CS, Meyer AA. Xenogeneic mouse fibroblasts persist in human cultured epidermal grafts: a possible mechanism of graft loss. *J Trauma* 1995; **39**: 75–9

T. Okano, Institute of Advanced Biomedical Engineering and Science, Tokyo Women's Medical University, 8-1 Kawada-cho, Shinjuku-ku, Tokyo, 162-8666, Japan.
e-mail: tokano@abmes.twmu.ac.jp

H&E, haematoxylin and eosin.

Micropatterned surfaces prepared using a liquid crystal projector-modified photopolymerization device and microfluidics

Kazuyoshi Itoga, Masayuki Yamato, Jun Kobayashi, Akihiko Kikuchi, Teruo Okano
Institute of Advanced Biomedical Engineering and Science, Tokyo Women's Medical University, CREST-JST, Kawada-cho 8-1, Shinjuku-ku, Tokyo 162-8666, Japan

Received 17 November 2003; accepted 20 November 2003
Published online 11 March 2003 in Wiley InterScience (www.interscience.wiley.com). DOI: 10.1002/jbm.a.30010

Abstract: A commercial liquid crystal device projector was modified for photopolymerization using its on-board intense light source and a precision optical control circuit. This device projects reduced images generated by a typical personal computer onto the stage where photopolymerization on a surface occurs. This all-in-one device does not require expensive photomasks and external light sources. However, light scattering and diffraction through glass substrates resulted in undesired reactions in areas corresponding to masked (black) domains in mask patterns, limiting pattern resolution. To overcome this shortcoming, two-step surface patterning was developed. First, three-dimensional microstructures of crosslinked silicone elastomer were fabricated with this device and adhered onto silanized glass substrate surfaces, forming microchannels in patterns on the glass support. Then, acrylamide monomer solution containing photoreactive initiator was flowed into these micromold channels and reacted *in situ*. The resultant polyacrylamide layer was highly hydrophilic and repelled protein adsorption. Cell seeding on these patterns in serum-supplemented culture medium produced cells selectively adhered to different patterns: cells attached and spread only on unpolymerized silanized glass surfaces, not on the photopolymerized acrylamide surfaces. This technique should prove useful for inexpensive, rapid prototyping of surface micropatterns from polymer materials. © 2004 Wiley Periodicals, Inc. J Biomed Mater Res 69A: 391–397, 2004

Key words: liquid crystal projector; mask-less pattern formation; microfluidics; cell pattern; cell culture; polydimethylsiloxane (PDMS); polyacrylamide

INTRODUCTION

Soft lithography, first proposed by Whitesides et al.,[1–3] has been widely used for surface micropatterning and other applications. Microstamps for soft lithography templates, usually made of polydimethylsiloxane (PDMS), are conventionally fabricated by semiconductor microfabrication techniques, in which the lithographic preparation of photomask masters is often time-consuming and expensive. Laser ablation is also utilized for the preparation of microstamps,[4,5] and is also less inexpensive. Photopolymerization with standard transparency sheets on which mask patterns were printed by laser printers is another convenient method.[6–9] However, expensive high-end laser printers are required to achieve higher resolution.

Correspondence to: T. Okano; e-mail: tokano@abmes.twmu.ac.jp

Contract grant sponsor: Japan Society for the Promotion of Science; contract grant number: 13308055.
Contract grant sponsor: the Promotion and Mutual Aid Corporation for Private School of Japan, Grants-in-Aid for Scientific Research.

We previously reported a novel photopolymerization device modified from a conventional liquid crystal device projector (LCDP) having an intense light source and precise optical circuit controls.[10] Recent liquid crystal device (LCD) innovation realizes large-scale high-density liquid crystal panels with micrometer scale resolution. The typical pixel size is approximately 20 μm. Such resolution can be useful for micropatterning surfaces in biomedical fields. Furthermore, LCDPs have a well-controlled light source. Projection images can be easily generated using a personal computer (PC) without any special software. Herein, we show preparation of micromolds made of PDMS and surface micropatterning by LCDP photopolymerization utilizing microfluidics. The LCDP-modified device was exploited as a light source and readily accessible photopatterning capabilities.

MATERIALS AND METHODS

Materials

Methacrylate-modified reactive silicone (X-22-164A) was kindly provided by Shin-Etsu Chemical Co. (Tokyo,

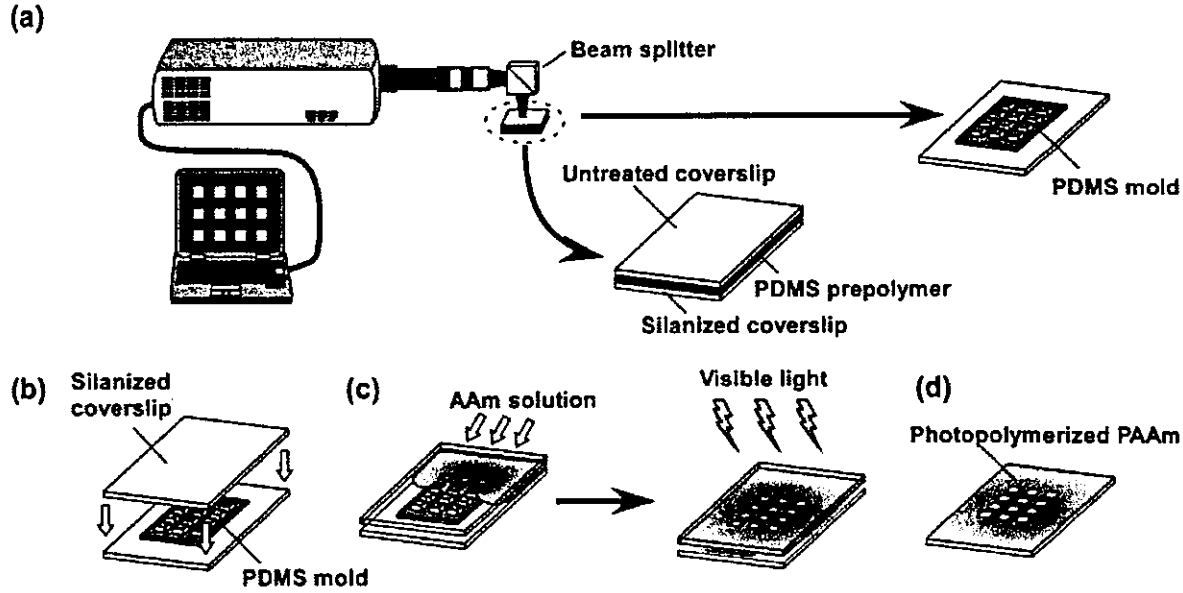

Figure 1. Two-step surface micropatterning utilizing the LCDP-modified photopolymerization device. Three-dimensional PDMS microstructures were prepared for microfluidics patterning on silanized glass surfaces. Micromolded PDMS photopolymerization utilized the LCDP-modified device with designated patterns (a). PDMS microstructures were then placed in contact with silanized glass surfaces as a patterned channel mold (b). Through the mold's open microstructures on the glass surface, acrylamide (AAm) monomer was applied to the coverslip surface, and then LCD light was irradiated with the LCDP-modified device in PC-generated patterns (c). Only in the noncontact PDMS open channel regions, photopolymerization of AAm occurred so that surface micropatterning with PAAm could be achieved (d). Wherever PDMS microstructures contacted the surface, no AAm photopolymerization was observed.

Japan). 3-Methacryloxypropyltrimethoxysilane (MPTMS; Shin-Etsu Chemical Co.), anhydrous methanol (Kanto Chemical Co., Tokyo, Japan), acrylamide, *N,N*-dimethylformamide (DMF), (±)-camphorquinone, *N,N*-dimethyl-*p*-toluidine, anhydrous 1,4-dioxane (Wako Pure Chemical Industries Ltd., Osaka, Japan), fluorescein isothiocyanate (FITC)-labeled bovine serum albumin, rhodamine 123 (both Sigma-Aldrich, St. Louis, MO), and all other chemicals were used as received.

Silane functionalization of glass surfaces

Both sides of glass coverslips (0.2 mm in thickness; Matsunami Glass Inc., Osaka, Japan) were treated by oxygen plasma (irradiation intensity: 400 W; oxygen pressure: 0.1 mmHg) for 180 s in a plasma dry cleaner (PX-1000; SAMCO International, Kyoto, Japan) to clean the surfaces. Plasma-treated coverslips were placed in a separable flask, and dried under vacuum for 30 min. Ten milliliters of MPTMS and 500 mL of anhydrous methanol were poured into the flask under nitrogen gas flow. The coupling reaction of MPTMS with clean, dry coverslip surfaces proceeded under reflux for 24 h at 60°C. The modified coverslips were rinsed repeatedly with methanol and distilled water, and dried for 24 h at 70°C.

Surface micropatterning with polyacrylamide (PAAm) by LCD photopolymerization in PDMS molds

First, surface patterning of PDMS derivatives on the coverslip was performed by irradiation of visible light through patterned images on the liquid crystal panel. A typical preparation procedure follows: camphorquinone (10 mg) as a photopolymerization initiator, and *N,N*-dimethyl-*p*-toluidine (1.0 μL) as a photosensitizer were dissolved in 1.00 g of methacrylate-modified reactive silicone. The solution (6.0 μL) was dropped onto the MPTMS-immobilized coverslip (24 × 24 mm), then covered with an untreated coverslip, creating a liquid film spread uniformly between the coverslips. The set of coverslips was placed in the LCDP apparatus with the untreated coverslip face-forward toward the light source. Visible light LCDP irradiation was performed directly through the top of the untreated coverslip for 20 min. After irradiation, the untreated coverslip was stripped off from the microfabricated PDMS-immobilized on the MPTMS-immobilized coverslip [see Fig. 1(a)]. The resulting PDMS-micropatterned coverslip was repeatedly washed with 1,4-dioxane and acetone to remove unreacted PDMS oligomers.

Second, acrylamide (0.20 g), camphorquinone (10 mg) as the photopolymerization initiator, and *N,N*-dimethyl-*p*-toluidine (1.0 μL) as a photosensitizer were dissolved in 0.80 g of DMF. The MPTMS-immobilized coverslip was then covered with the PDMS-micropatterned coverslip [see Fig. 1(b)],

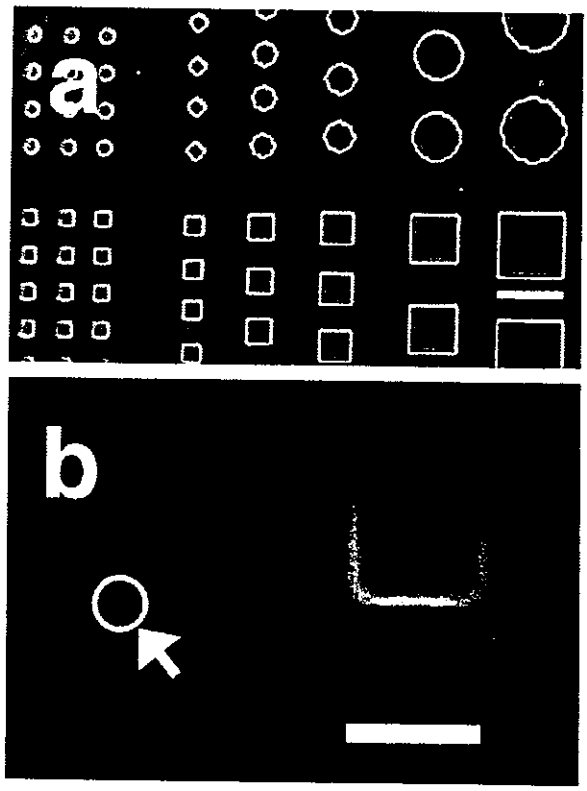

Figure 2. Phase contrast microscopy of three-dimensional PDMS stamp microstructures produced by LCD photopolymerization through the PC-generated mask. Note small gaps among square dots (arrow) caused by the LCD pixel wiring shadows. Scale bar: 200 μm (a); 50 μm (b).

forming patterned microchannels between the two apposing surfaces. The acrylamide solution was poured into the gap of the contacting coverslips and the set of coverslips was irradiated by visible light under a brightness of approximately 50,000 luxes for 4 min [see Fig. 1(c)]. After irradiation, the PDMS-micropatterned coverslip was stripped off, leaving the microfabricated PAAm photoimmobilized on the

Figure 3. SEM of three-dimensional PDMS microstructures. Scale bar: 100 μm.

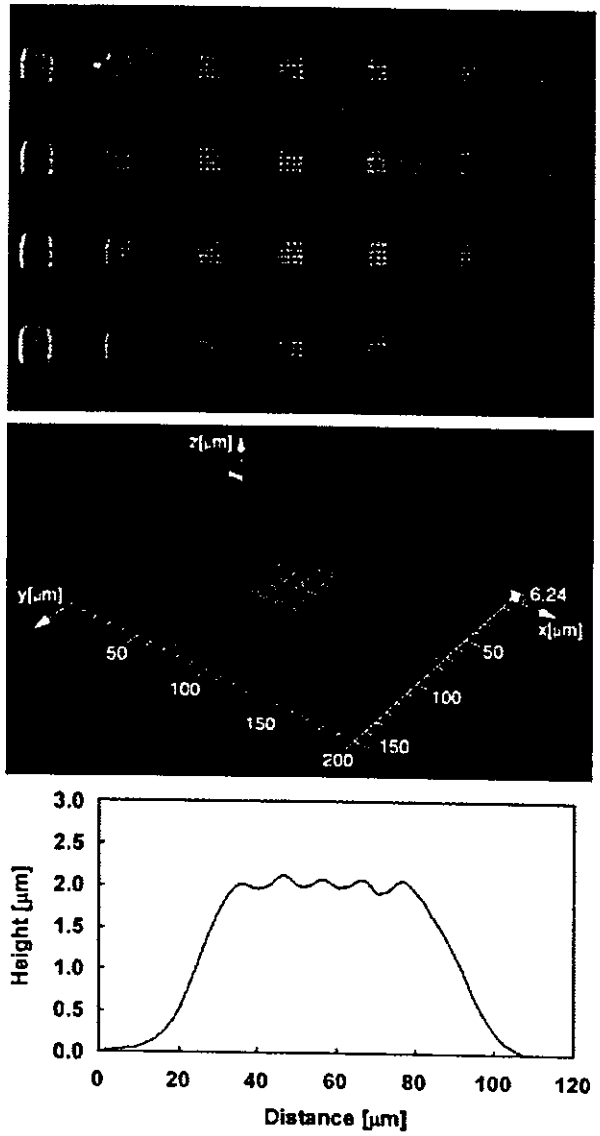

Figure 4. Three-dimensional profiles of three-dimensional PDMS microstructures from laser scanning confocal imaging. Scale bar: 100 μm.

MPTMS-immobilized coverslip in patterns determined by the PDMS micromold. The resulting PAAm-micropatterned coverslip was repeatedly washed with acetone to remove unreacted chemicals.

Micropatterned surfaces were examined under a phase contrast microscope (TE300; Nikon, Tokyo, Japan). Three-dimensional profiles of the surfaces were obtained by reflective confocal laser scanning microscopy (ICM-1000; Leica Microsystems, Wetzlar, Germany). For scanning electron microscopy (SEM) imaging (S-800; Hitachi, Tokyo, Japan), micropatterned surfaces were deposited with a thin conducting gold sputtered layer. Atomic force microscope (AFM) images of patterned PAAm surfaces were obtained with a scanning probe microscope (SPM-9500J3; Shimadzu Corp., Kyoto, Japan) that was operated in dynamic mode in distilled water at ambient temperature.

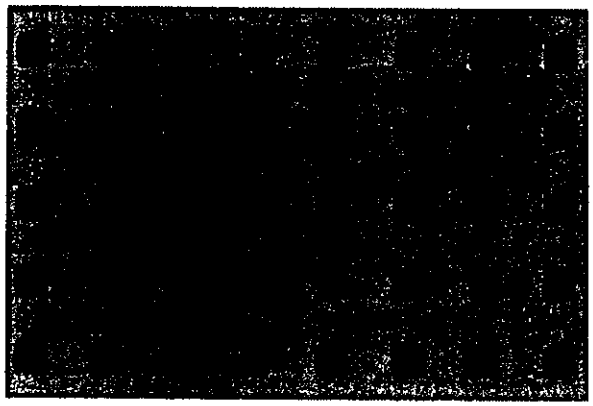

Figure 5. Microfluidic fidelity testing with three-dimensional PDMS microstructures. Fluorescent dye solution (1% rhodamine 123 in DMF) was poured onto the mold-glass sandwiched surface and observed under a microscope. No leaks were detected over all surfaces observed, reflecting high fidelity of pattern size and surface contact. Scale bar: 100 μm. [Color figure can be viewed in the online issue, which is available at www.interscience.wiley.com.]

Protein adsorption

FITC-labeled bovine serum albumin was dissolved in Dulbecco's phosphate buffered saline (PBS) at a concentration of 250 μg/mL. A few drops of the protein solution were distributed onto the PAAm-micropatterned surfaces and stored wet at room temperature overnight. The patterned surfaces were rinsed with PBS and water, and then directly examined under a fluorescence microscope (TE300; Nikon).

Cell culture

Bovine aortic endothelial cells (JCRB0099) were provided from Japan Health Science Foundation and cultured in Dulbecco's modified Eagle minimum essential medium (DMEM) supplemented with 10% fetal bovine serum (FBS), 100 U/mL penicillin and 100 μg/mL streptomycin. Cells were recovered from tissue culture polystyrene dishes by treatment with 0.05% trypsin/0.05% ethylenediaminetetraacetic acid in PBS and were routinely split at a ratio of 1:4 and carried in DMEM supplemented with 10% FBS, 100 U/mL penicillin, and 100 μg/mL streptomycin. Endothelial cells (5.0×10^4 cells/mL) were seeded onto treated glass coverslips. Cell morphology in culture on patterned surfaces was monitored under a phase contrast microscope (TE300; Nikon).

RESULTS

In the present study, reliable surface micropatterning to produce cell-surface manipulations was achieved in two steps (shown in Fig. 1). First, three-

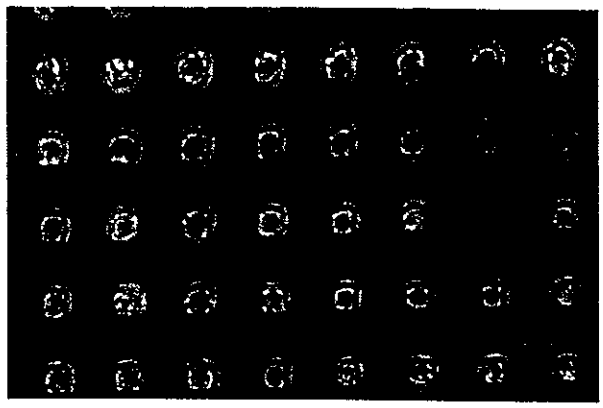

Figure 6. Water condensation patterns on PAAm-micropatterned surfaces seen in phase contrast microscopy. Scale bar: 100 μm.

dimensional molded microstructures were prepared with PDMS on silanized glass surfaces by photopolymerization utilizing the LCDP-modified device. In the modified LCDP used in the present study, light from the lamp passed through liquid crystal panels was downsized by the projector lens, turned by the beam splitter downward, and irradiated onto the sample stage, whose position was monitored and controlled for focus adjustment. The LCDP used here has three liquid crystal panels each comprising 480,000 pixels (800×600, 1.78 cm in diagonal). Each square pixel has sides of 18 μm reduced through the projection lens optics. In the present study, the reduced individual pixel size was fixed to 10 μm, so that the final projection area was 8×6 mm. Mask patterns were generated on a typical PC with commercially available software such as Microsoft Word® and Microsoft PowerPoint®. Identical images appearing on the PC monitor were projected onto the sample stage in a reduced size. After photopolymerization, the resultant

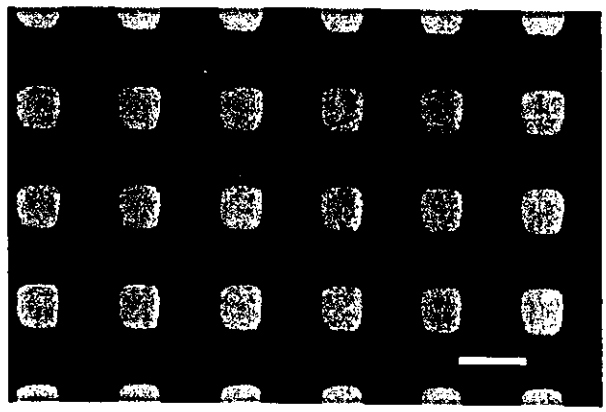

Figure 7. FITC-albumin adsorption on PAAm-micropatterned surfaces detected with fluorescent microscopy. Scale bar: 100 μm. [Color figure can be viewed in the online issue, which is available at www.interscience.wiley.com.]

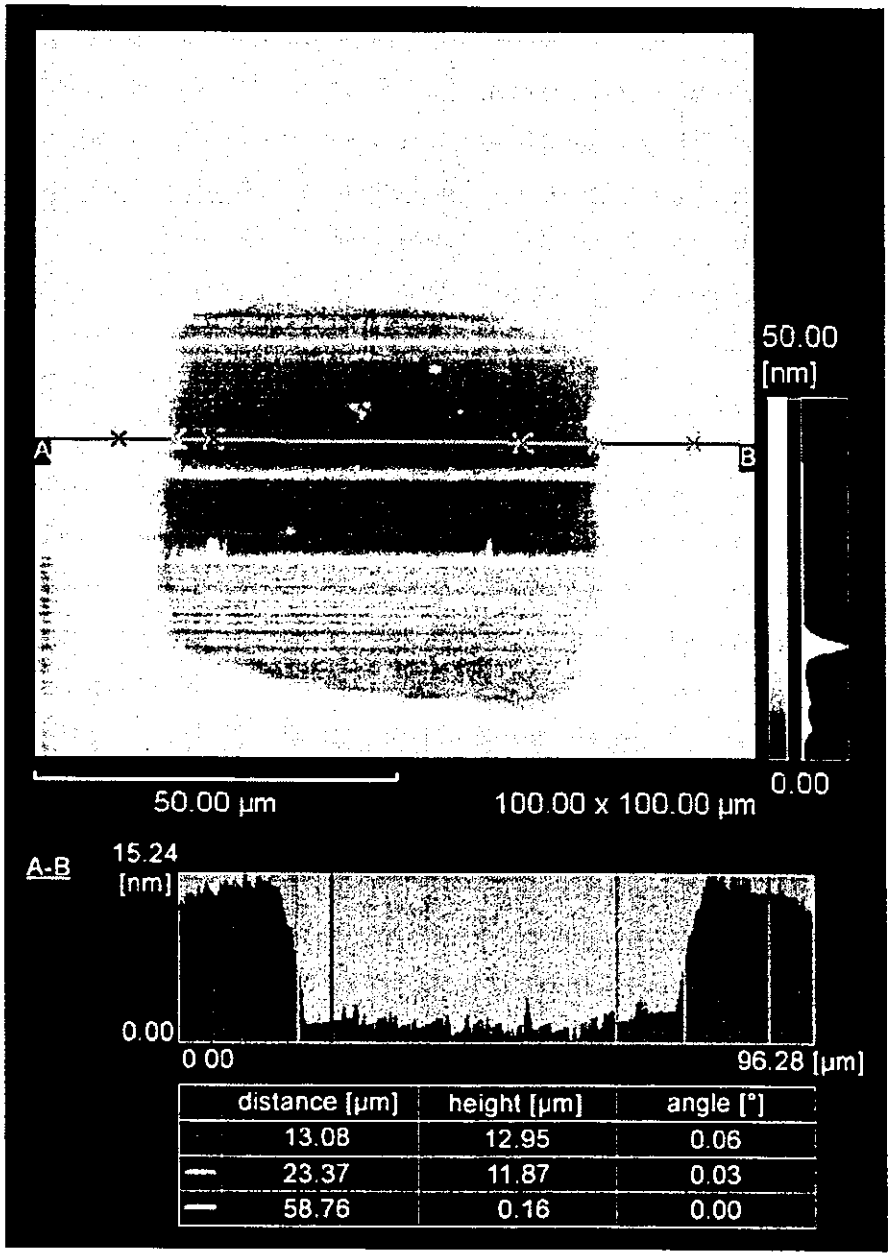

Figure 8. Three-dimensional profiles of wet PAAm-micropatterned surfaces observed with AFM.

three-dimensional PDMS microstructures are easily observed under a phase contrast microscope (see Fig. 2) as well as by SEM (shown in Fig. 3). Three-dimensional topological profiles were obtained with a reflective confocal laser scanning microscope (images shown in Fig. 4). As these imaging methods show, high fidelity to the computer-generated mask patterns was consistently achieved. The convex and concave domains corresponded to white and black domains on PC-generated images, respectively. Under the present conditions, the depth of concave domains is approximately 2 µm, but the sectional sidewall profile was trapezoidal. The top had the same dimension as the PC-generated images, whereas the base of the structure formed was slightly larger. This is likely caused by LCD light scattering and/or diffraction. Each micropattern comprised small square dots having 10-µm sides. Because of shading from LCD wires aligned between pixels on the liquid crystal panel to switch each pixel on and off, small submicron gaps were formed by LCD exposure among square dots [arrow in Fig. 2(b)].

These three-dimensional PDMS microstructures were directly pressed onto another silanized glass sur-

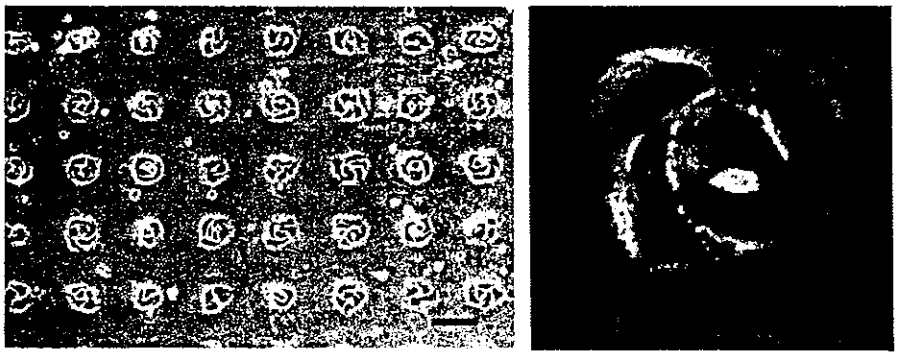

Figure 9. Cell manipulation on PAAm-micropatterned surfaces (phase contrast microscope image after culture in 10% FBS-DMEM for 19 days). Scale bar: 100 μm (left); 50 μm (right).

face, forming molded patterned channels on contact for microfluidics purposes. To confirm tight contact of PDMS microstructures on these glass surfaces, rhodamine DMF dye solution was flowed around these contacts and observed under a microscope (shown in Fig. 5). No leaks were detected over the entire surfaces observed, so that quite a sharp, fluid-tight boundary between the concave and convex PDMS domains was obtained. Acrylamide monomer solution was then poured through these concave microstructures, and light was irradiated. Photopolymerization of acrylamide occurred only in the concave-molded domains, so that surface micropatterning with hydrophilic PAAm could be achieved using the patterned PDMS template. After polymerization of PAAm, the resultant polymer micropattern was not detected under a phase contrast microscope, but the surface micropatterning was visualized by two other ways. First, water vapor condensation was observed only on non-PDMS contact areas under a humid atmosphere (see Fig. 6). Because silanized glass surfaces are hydrophobic, condensation is expected to occur selectively on hydrophilic PAAm surfaces.[11] Second, FITC-albumin adsorption was observed only in the areas contacted directly by the PDMS convex patterns during acrylamide photopolymerization (see Fig. 7). Hydrophilic PAAm surfaces are known to repel protein adsorption,[12,13] consistent with these observations and pattern fidelity. Wet PAAm layer thickness was determined to be approximately 12 nm by AFM (see Fig. 8).

On the micropatterned surfaces, endothelial cells specifically adhered to patterned areas where the PDMS convex domains contacted the silanized surface, that is, where PAAm could not flow or be photografted (see images in Fig. 9). Such site-selective cell adhesion was achieved even in the presence of 10% FBS media. Consistently, on the areas not in contact with the PDMS patterns (i.e., channel domains where PAAm was grafted), cell adhesion was completely inhibited. The cell micropattern fidelity was maintained intact for more than 1 month even in the presence of serum (data not shown). Cytotoxicity was not observed during this culture (data not shown).

DISCUSSION

In our previous study, one-step LCD micropatterning of surfaces by grafting with polyethylene glycol was reported.[10] Liquid crystal panels equipped in the projector can completely shield emitted light to pattern at high line resolution. However, irradiated light can be diffracted or scattered on the glass surface substrate and diffused through the glass. Therefore, polyethylene glycol was found to be grafted even on black (unexposed) domains in PC-generated images. To eliminate the effect of light diffraction and scattering for more precise control of surface micropatterning, two-step micropatterning has been developed here. Because the PDMS molds exhibited tight contacts with silanized glass surfaces, no liquid leakage was observed from the microfluidic tests of sealing. Therefore, a high fidelity of final PAAm micropatterns with the top surface image transfer from the PDMS molds was obtained.

Under the present conditions, the resultant PAAm layers were highly hydrophilic and able to repel protein adsorption (see Fig. 7). On the contrary, silanized glass surfaces allowed cell adhesion in culture medium supplemented with serum even without precoating extracellular matrix proteins such as fibronectin, typically required for cell adhesion on hydrophobic surfaces. As a result, selective cell adhesion at high pattern fidelity was achieved by cell seeding on micropatterned surfaces in the presence of serum (Fig. 9).

Micropatterned surfaces were fabricated easily and quickly with the present LCD device without any need for expensive pattern mask masters, an additional light source, or other optics. Even with the present typical LCDP, requisite pattern fidelity and

resolution for many biomedical applications is readily achievable. Recent progress in improved high resolution and high-density LCDP will facilitate much finer micropatterning required for more advanced applications. The present device has both a liquid crystal panel imaging PC-generated patterns and an intense light source. Such an all-in-one device should be useful for the preparation of micropatterned surfaces for biomedical applications and other microfluidics surfaces in a rapid prototyping manner.

The authors appreciate the useful comments and technical criticism from Prof. D. W. Grainger (Colorado State University, Fort Collins, CO). The authors are grateful to Mr. Masao Matsuda of Shimadzu Corporation for AFM experiments, and are thankful for the cooperation of Digital Systems Development Center of Sanyo Electric Co., Ltd.

References

1. Xia Y, Whitesides GM. Soft lithography. Angew Chem Int Ed Engl 1998;37:550–575.
2. Whitesides GM, Ostuni E, Takayama S, Jiang X, Ingber DE. Soft lithography in biology and biochemistry. Annu Rev Biomed Eng 2001;3:335–373.
3. Michel B, Bernard A, Bietsch A, Delamarche E, Geissler M, Juncker D, Kind H, Renault J-P, Rothuizen H, Schmid H, Schmidt-Winkel P, Stutz R, Wolf H. Printing meets lithography: soft approaches to high-resolution patterning. IBM J Res Dev 2001;45:697–719.
4. Grzybowski BA, Haag R, Bowden N, Whitesides GM. Generation of micrometer-sized patterns for microanalytical applications using a laser direct-write method and microcontact printing. Anal Chem 1998;70:4645–4652.
5. Wolfe DB, Ashcom JB, Hwang JC, Schaffer CB, Mazur E, Whitesides GM. Customization of poly(dimethylsiloxane) stamps by micromachining using a femtosecond-pulsed laser. Adv Mater 2003;15:62–65.
6. Qin D, Xia Y, Whitesides GM. Rapid prototyping of complex structures with feature sizes lager than 20 μm. Adv Mater 1996;8:917–919.
7. McDonald JC, Whitesides GM. Poly(dimethylsiloxane) as a material for fabricating microfluidic devices. Acc Chem Res 2002;35:491–499.
8. Beebe DJ, Moore JS, Bauer JM, Yu Q, Liu RH, Devadoss C, Jo B-H. Functional hydrogel structures for autonomous flow control inside microfluidic channels. Nature 2000;404:588–590.
9. Wong JY, Velasco A, Rajagopalan P, Pham Q. Directed movement of vascular smooth muscle cells on gradient-compliant hydrogels. Langmuir 2003;19:1908–1913.
10. Itoga K, Yamato M, Kobayashi J, Kikuchi A, Okano T. Cell micropatterning using photopolymerization with a liquid crystal device commercial projector. Biomaterials 2004;25(11):2047–2053.
11. Ionov L, Minko S, Manfred Stamm M, Gohy J-F, Jérôme R, Scholl A. Reversible chemical patterning on stimuli-responsive polymer film: environment-responsive lithography. J Am Chem Soc 2003;125:8302–8306.
12. Bearinger JP, Castner DG, Golledge SL, Rezania A, Hubchak S, Healy KE. P(AAm-*co*-EG) interpenetrating polymer networks grafted to oxide surfaces: surface characterization, protein adsorption, and cell detachment studies. Langmuir 1997;13:5175–5183.
13. Saito N, Matsuda T. Protein adsorption on self-assembled monolayers with water-soluble non-ionic oligomers using quartz-crystal microbalance. Mater Sci Eng C 1998;6:261–266.

Langmuir **2004**, *20*, 5506−5511

Ultrathin Poly(*N*-isopropylacrylamide) Grafted Layer on Polystyrene Surfaces for Cell Adhesion/Detachment Control

Yoshikatsu Akiyama,† Akihiko Kikuchi,† Masayuki Yamato,† and Teruo Okano*,†

Institute of Advanced Biomedical Engineering and Science, COE Program for 21st Century, Tokyo Women's Medical University, 8-1 Kawadacho, Shinjuku-ku, Tokyo 162-8666, Japan

Received November 14, 2003. In Final Form: April 12, 2004

We investigated physicochemical properties of two types of poly(*N*-isopropylacrylamide) (PIPAAm)-grafted tissue culture polystyrene (TCPS) surfaces, to elucidate the influential factors for thermally regulated cell adhesion and detachment to PIPAAm-grafted surfaces. The two types of PIPAAm-grafted surfaces were prepared by the electron beam polymerization method. Attenuated total reflection Fourier transform infrared spectroscopy revealed that amounts of the grafted polymers were $1.4 \pm 0.1\ \mu g/cm^2$ for PIPAAm-1.4 and $2.9 \pm 0.1\ \mu g/cm^2$ for PIPAAm-2.9. Both PIPAAm-grafted surfaces showed hydrophobic/hydrophilic property alterations in response to temperature. However, PIPAAm-1.4 surfaces were more hydrophobic ($\cos\theta = 0.21$ at 37 °C and $\cos\theta = 0.35$ at 20 °C) than PIPAAm-2.9 ($\cos\theta = 0.42$ at 37 °C and $\cos\theta = 0.50$ at 20 °C) both above and below the PIPAAm's transition temperature. Thicknesses of the grafted PIPAAm layers were estimated to be 15.5 ± 7.2 nm for PIPAAm-1.4 and 29.5 ± 8.4 nm for PIPAAm-2.9, by the use of UV excimer laser and atomic force microscope. Bovine carotid artery endothelial cells (ECs) adhere to the surfaces of PIPAAm-1.4 and proliferate to form confluent cell monolayers. The cell monolayers were harvested as single cell sheets by temperature decrease from 37 to 20 °C. On the contrary, ECs did not adhere to the surfaces of PIPAAm-2.9. This phenomenon was correlated with an adsorption of cell adhesion protein, fibronectin, onto surfaces of PIPAAm-1.4 and -2.9. In the case of nano-ordered thin grafted surfaces, the surface chain mobility is strongly influenced by the thickness of PIPAAm grafted layers because dehydration of PIPAAm chains should be enhanced by the hydrophobic TCPS surfaces. PIPAAm graft amounts, that is, thickness of the PIPAAm grafted layers, play a crucial role in temperature-induced hydrophilic/hydrophobic property alterations and cell adhesion/detachment behavior.

Introduction

We have been carrying out the preparation of thermoresponsive polymer-modified surfaces with designated molecular configuration at the interfaces.[1-3] Thermoresponsive polymers poly(*N*-isopropylacrylamide) (PIPAAm) and its derivatives are used as the surface modifiers.[1-3] These surfaces are utilized to propose new chromatographic separation methods for a variety of types of bioactive compounds in a sole aqueous mobile phase.[4-6] We further applied the thermoresponsive surfaces for thermally regulated cell adhesion and detachment[7-9] and extended the idea to tissue engineering.[10-13] Confluently cultured cell monolayers on hydrophobized PIPAAm-modified surfaces at 37 °C detach as single cell sheets by lowering the culture temperature to 20 °C where the modified surfaces become hydrophilic due to PIPAAm's hydration/dehydration transition at 32 °C. In our preliminary studies, graft amounts of PIPAAm on the surfaces have significant influence on cell adhesion behavior.[14,15] However, detailed mechanisms to explain why cells cannot adhere on the surfaces with high amounts of grafted PIPAAm chains are unclear. Such phenomenon was also found for PIPAAm dip-coated surfaces or PPAAm hydrogels.

In the present paper, we focused on the correlation of the thickness of PIPAAm covalently grafted layers on tissue culture polystyrene (TCPS) surfaces and cell adhesion/detachment behavior. For this purpose, we utilized limited excimer laser ablation and atomic force microscopic methods to determine the thickness of PIPAAm grafted layers. Preliminary ellipsometry measurement did not work to determine the grafted layer thickness, since the refractive indices are similar for polystyrene and PIPAAm. Then, we investigated thermoresponsive

* Corresponding author. Phone: +81-3-3353-8111 ext. 30233. Fax: +81-3-3359-6046. E-mail: tokano@abmes.twmu.ac.jp.

† Core Researches for Evolutional Science and Technology (CREST), Japan Science and Technology Agency.

(1) Takei, Y. G.; Aoki, T.; Sanui, K.; Ogata, N.; Sakurai, Y.; Okano, T. *Macromolecules* **1994**, *27*, 6163−6166.

(2) Yakushiji, T.; Sakai, K.; Kikuchi, A.; Aoyagi, T.; Sakurai, Y.; Okano, T. *Langmuir* **1998**, *14*, 4657−4662.

(3) Kikuchi, A.; Okano, T. *Prog. Polym. Sci.* **2002**, *27*, 1165−1193.

(4) Kanazawa, H.; Yamamoto, K.; Matsushima, Y.; Takai, N.; Kikuchi, A.; Sakurai, Y.; Okano, T. *Anal. Chem.* **1996**, *68*, 100−105.

(5) Kanazawa, H.; Kashiwase, Y.; Yamamoto, K.; Matsushima, Y.; Kikuchi, A.; Sakurai, Y.; Okano, T. *Anal. Chem.* **1997**, *69*, 823−830.

(6) Kanazawa, H.; Sunamoto, T.; Matsushima, Y.; Kikuchi, A.; Sakurai, Y.; Okano, T. *Anal. Chem.* **2000**, *72*, 5961−5966.

(7) Yamada, N.; Okano, T.; Sakai, H.; Karikusa, F.; Sakurai, Y. *Makromol. Chem. Rapid. Commun.* **1990**, *11*, 571−576.

(8) Okano, T.; Yamada, N.; Sakai, H.; Sakurai, Y. *J. Biomed. Mater. Res.* **1993**, *27*, 1243−1251.

(9) von Recum, H. A.; Kim, S. W.; Kikuchi, A.; Okuhara, M.; Sakurai, Y.; Okano, T. *J. Biomater. Sci., Polym. Ed.* **1998**, *9*, 1241−1254.

(10) Kushida, A.; Yamato, M.; Konno, C.; Kikuchi, A.; Sakurai, Y.; Okano, T. *J. Biomed. Mater. Res.* **2000**, *51*, 216−223.

(11) Shimizu, T.; Yamato, M.; Kikuchi, A.; Okano, T. *Tissue Eng.* **2001**, *7*, 141−151.

(12) Yamato, M.; Shimizu, T.; Harimoto, M.; Hirose, M.; Kushida, A.; Kwon O. H.; Kikuchi, A.; Okano, T. In *Tissue Engineering for Therapeutic Use 5*; Ikada, Y., Ohshima, N., Eds.; Elsevier Science: Amsterdam, 2001; pp 93−100.

(13) Yamato, M.; Okano, T. *Macromol. Chem. Symp.* **2001**, *14* (2), 21−29.

(14) Sakai, H.; Doi, Y.; Okano, T.; Yamada, N.; Sakurai, Y. In *Advanced Biomaterials in Biomedical Engineering and Drug Delivery Systems*; Ogata, N., Feijen, J., Kim, S. W., Okano, T., Eds.; Springer: Tokyo, 1996; pp 229−230.

(15) Yamato, M.; Konno, C.; Koike, S.; Isoi, Y.; Shimizu, T.; Kikuchi, A.; Makino, K.; Okano, T. *J. Biomed. Mater. Res.* **2003**, *67A*, 1065−1071.

10.1021/la036139f CCC: $27.50
Published on Web 05/26/2004

cellular adhesion/detachment on the prepared surfaces to discuss the influence of the grafted layer thickness on the cellular behavior on these modified surfaces.

Experimental Section

Preparation of the PIPAAm-Grafted TCPS Dishes. PIPAAm-grafted surfaces were prepared as reported previously.[4] In brief, *N*-isopropylacrylamide (IPAAm) monomer, a kind gift from Kohjin (Tokyo, Japan), was dissolved in 2-propanol at concentrations of 55 and 80 wt %. Solution (30 μL) was added and spread uniformly over TCPS surfaces (Falcon 3001, BD Bioscience, Billerica, MA) These dishes were immediately subjected to irradiation with a 0.25 MGy electron beam, using an Area Beam Electron Processing System (Nissin High Voltage, Kyoto, Japan). PIPAAm-grafted dishes were washed extensively with cold distilled water to remove unreacted IPAAm monomer and ungrafted PIPAAm.

Preparation of PIPAAm-Grafted Gel on Glass Coverslips. IPAAm monomer (1.56 g), *N,N*-methylenebisacrylamide (27 mg), and ammonium peroxodisulfate (8.0 mg) were dissolved in distilled water (10 mL). The mixture was subject to N_2 bubbling for 10 min and then *N,N,N',N'*-tetramethylethylenediamine (48 μL) was added to the mixture. The mixture was immediately poured into the void space between two glass coverslips where a Teflon spacer (with 50 μm thickness) was placed. In advance, the coverslip surfaces were modified with 3-methacryloxypropyl trimethoxysilane after O_2 plasma treatment. Polymerization reaction for the glass coverslips containing the mixture was performed at 15 °C for 24 h, and the resulting grafted PIPAAm gel was washed extensively with distilled water.

UV Excimer Laser Ablation of PIPAAm-Grafted Surfaces. Irradiation of an ArF excimer laser (L5910 III B; Hamamatsu Photonics K.K., Shizuoka, Japan) was achieved onto PIPAAm-grafted surfaces by passing a laser pulse through an optical microscope, resulting in ablative photodecomposition. The excimer laser (193 nm) was irradiated at a laser fluence of either 10 or 20 mJ/cm^2 with a pulse width of 5 ns. The number of laser shots was changed from 1 to 9 onto the PIPAAm-grafted surfaces. Each ablated region was 30 μm × 25 μm.

Staining PIPAAm-Grafted Surfaces with Hydrophobic Fluorescent Dye, DiIC18. The laser-ablated surfaces were stained with 25 μg/mL 1,1'-dioctadecyl-3,3,3',3'-tetramethylindocarbocyanine perchlorate (DiIC18) (Molecular Probes Inc., Eugene, OR) in Dulbecco's phosphate-buffered saline (PBS; Sigma, St. Louis, MO) for 1 min at 23 °C. They were then washed extensively with PBS for five times. The surfaces were finally observed by fluorescent microscope. The fluorescence intensity of the ablated surfaces was evaluated by NIH image software (for the Macintosh, version 1.63).

Characterization. The amount of grafted PIPAAm was determined by attenuated total reflection Fourier transform infrared spectroscopy (ATR/FTIR, IR-470 Plus equipped with an ATR-300 H unit (Ge crystal with an incidence angle of 45°, and the number of reflection of 8; JASCO Co., Tokyo, Japan). As the base substrate was TCPS, an absorption arising from mono-substituted aromatic rings was observed at 1600 cm^{-1}. Absorption of amide carbonyl derived from PIPAAm grafts appeared in the region of 1650 cm^{-1}. The peak intensity ratio of I_{1650}/I_{1600} was used to determine the graft density of PIPAAm on the surfaces. A known PIPAAm amount cast on TCPS from solution was used for a calibration curve. Surface wettability was evaluated by measuring static contact angles (Image processing type CA-X, Kyowa Interface Science, Saitama, Japan) toward air bubbles in Milli-Q water. Atomic force microscopy (AFM) images were obtained with a NanoScope IIIa (Digital Instruments, Santa Barbara, CA) using Tapping Mode in air, for measuring the thickness of the grafted polymer layers. Prior to measurements, the central part of PIPAAm-grafted dishes was cut into a piece of 1 cm × 1 cm in size. The scan rate was 0.2 Hz, and the measurements were carried out with an AFM probe of NCHW type (NANOSENSORS, Germany). The rms (root-mean-square) value of the surface roughness of the image was determined with software supplied with the NanoScope IIIa. The thickness of the grafted polymer layers was determined from data of section profiles drawn in the AFM image. Time-of-flight secondary ion mass spectrometry (TOF-SIMS) images were obtained with a TOF-SIMS IV (Cameca Instruments, France) system in static mode. The dose of gallium ions used as the primary beam was 1.9 × 10^{13} ions/cm^2.

Cells and Cell Culture. Bovine endothelial cells (ECs; Health Science Research Resource Bank, Osaka, Japan) were cultured with Dulbecco's modified Eagle's medium (DMEM; IWAKI, Chiba, Japan) supplemented with 10% fetal bovine serum (FBS; MORGATE Co., Ltd., Bulimba, Australia), 100 units/mL penicillin, 100 μg/mL streptomycin, and 0.25 μg/mL fungizone at 37 °C in a humidified atmosphere with 5.0% CO_2. ECs were recovered from normal TCPS dishes by treatment with 0.25% trypsin–2.65 mM EDTA (GIBCO BRL Life Technologies, Grand Island, NY) in PBS and seeded on PIPAAm-grafted dishes having different PIPAAm graft densities and TCPS dishes as the reference at 1.3 × 10^4 cells/cm^2. Cell morphology was photographed under a phase contrast microscope (TE300, Nikon, Tokyo, Japan).

Fibronectin Adsorption onto PIPAAm-Grafted Surfaces. Bovine plasma fibronectin (FN; Biomedical Technology Inc., Stoughton, MA) was adsorbed onto the PIPAAm-grafted surfaces by incubation of 10 μg/mL FN in PBS solution at 37 °C for 6 h. These dishes were then vigorously washed with PBS for five times. They were then blocked with 0.1% bovine serum albumin (BSA) in PBS for 1 h and reacted with 2.0 mg/mL rabbit polyclonal anti-bovine FN antibody (Biogenesis, Inc., Poole, U.K.) at a 1:200 dilution (final concentration, 10 μg/mL) for 2 h at 23 °C. Following five washes with PBS containing 0.1% BSA, they were incubated for an additional 1 h with 3.0 mg/mL FITC-conjugated goat anti-rabbit IgG antibody (CHEMICON International, Inc., Temecula, CA) with a 1:200 dilution (final concentration, 15 μg/mL) and again washed vigorously with 0.1% BSA in PBS for five times. The stained dishes were observed with a fluorescent microscope (TE2000-U, Nikon). After adsorption of FN molecules, the FN solution was collected and the concentration of FN was estimated by the micro BCA assay method (PIERCE Biotechnology, Inc., Rockford, IL). Amounts of adsorbed FN on PIPAAm-1.4, PIPAAm-2.9, and control TCPS surfaces were estimated from the calibration curve.

Results

Characterization of PIPAAm-Grafted Surfaces. Here, two types of PIPAAm-grafted TCPSs were evaluated for graft amounts of the PIPAAm surfaces and their thermoresponsive wettability changes. The grafted polymer amounts on two PIPAAm-grafted surfaces were determined from ATR/FTIR measurements and were 1.4 ± 0.1 μg/cm^2 (n = 4) and 2.9 ± 0.1 μg/cm^2 (n = 4), respectively. Those two surface types are abbreviated as PIPAAm-1.4 and PIPAAm-2.9, respectively, hereafter. Surface wettability of PIPAAm-1.4 and -2.9 was altered with temperature, as cos θ = 0.21 ± 0.01 (θ = 77.9 ± 0.60°) (n = 3) for PIPAAm-1.4 and cos θ = 0.35 ± 0.02 (θ = 69.5 ± 1.20°) (n = 3) for PIPAAm-2.9 at 37 °C changed to cos θ = 0.42 ± 0.02 (θ = 65.2 ± 1.20°) (n = 3) for PIPAAm-1.4 and cos θ = 0.50 ± 0.01 (θ = 60.0 ± 0.06°) (n = 3) for PIPAAm-2.9 at 20 °C.

Grafted PIPAAm Layers on TCPS Surfaces by UV Laser Ablation. PIPAAm-grafted TCPS surfaces were ablated with the UV excimer laser until the TCPS region was exposed for the following measurement of the graft layer thickness by means of atomic force microscopy. The ablated domains were stained with a hydrophobic fluorescent dye, DiIC18, to see whether the hydrophobic TCPS regions were exposed. Fluorescence of ablated domains was scarcely seen at one laser shot (Figure 1a). By sharp contrast, the fluorescent dye selectively stained the ablated domains clearly with increasing number of laser shots. The fluorescent intensity for PIPAAm-1.4 is likely to be saturated with 6 laser shots as shown in Figure 1b. This result indicates that the TCPS region is successfully exposed by 6 times of the laser ablation.

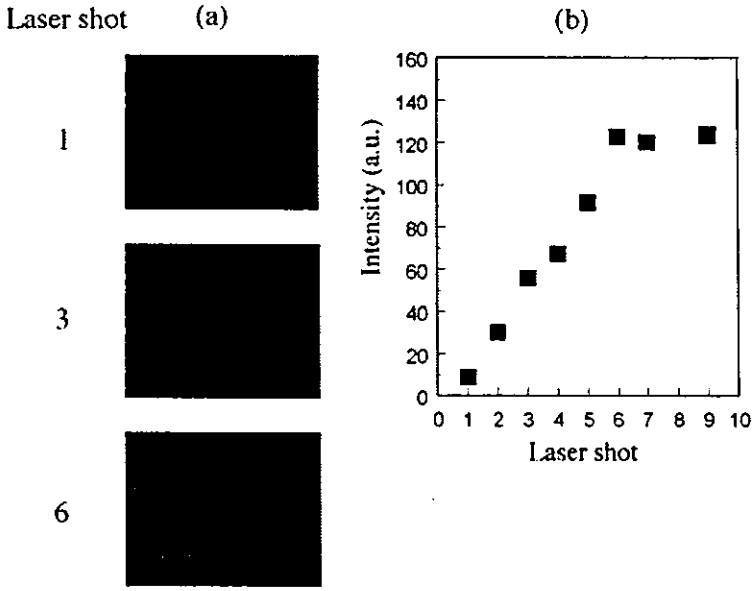

Figure 1. Fluorescence images of the domains on PIPAAm-1.4 surfaces stained by DiIC18 after the UV laser ablation at the number of 1, 3, and 6 laser shots (a) and fluorescence intensity of the domain as a function of the number of UV excimer laser shots (b). The numbers inserted in the fluorescent images correspond to the number of the laser shot. The laser fluence for the squares was 10 mJ/cm^2.

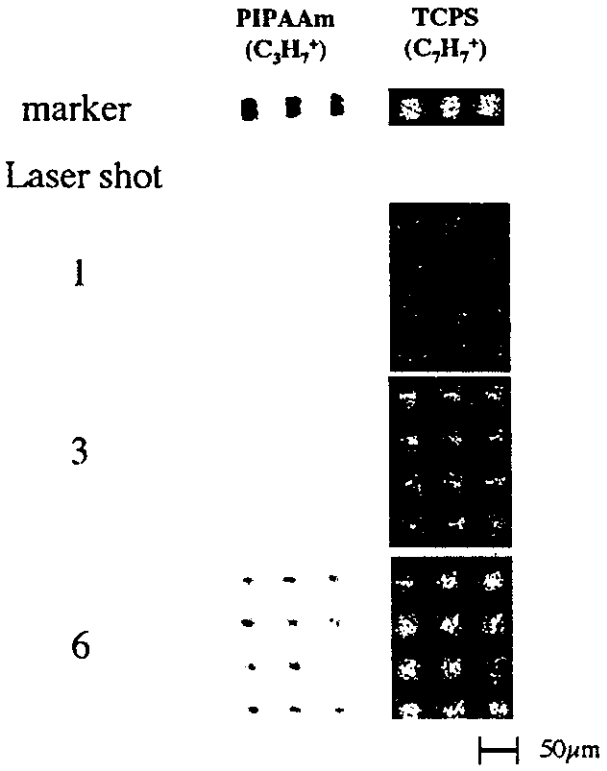

Figure 2. TOF-SIMS images displayed the spatial distribution of $C_3H_7^+$ (left) and $C_7H_7^+$ species (right) on PIPAAm-1.4 surfaces after the UV laser ablation at the number of 1, 3, and 6 laser shots. These images correspond to the images shown in Figure 1a. The $C_3H_7^+$ and $C_7H_7^+$ are characteristic of ion fragments derived from PIPAAm and TCPS composition, respectively. The laser fluence for the marker areas in the images was 50 mJ/cm^2.

Such a gradual exposure of TCPS was further confirmed by TOF-SIMS measurements (Figure 2). $C_3H_7^+$ ion was used to assign PIPAAm isopropyl side groups, and $C_7H_7^+$ ion was for phenyl groups of TCPS. In the left column of Figure 2, the entire surface was in bright color except the marker regions at laser shot of 1. With increasing laser shots, darker regions were seen in $C_3H_7^+$ ions. Such regions were brighter as $C_7H_7^+$ ion species were chosen in the TOF-SIMS images (right column in Figure 2).

Likewise, the ablated areas were stained with the fluorescent dye on PIPAAm-2.9 surfaces after the laser ablation. A stronger laser fluence was necessary for staining the regions (Figure 3), while such images were not obtained at a laser shot of 1 or 2 (data not shown). The stronger fluence should be due to the different amount and thickness of the grafted PIPAAm layers. The fluorescence intensity saturation at the laser shot of 3 also indicates that the TCPS region is completely revealed at this condition.

Measurement of Thickness of PIPAAm Layers by AFM. Figure 4 shows AFM images and their section profiles of the ablated domains for PIPAAm-1.4 (a) and for PIPAAm-2.9 (b). The PIPAAm-1.4 surface was relatively smooth, and ablated areas were clearly observed. This is sharp contrast with the relatively rough PIPAAm-2.9 surface. The rms values of PIPAAm-1.4 and -2.9 surfaces before the laser ablation were approximately 7.7 and 16.5 nm (data not shown), while those of the nonablated area in Figure 4a,b were ca. 6.0 and 17.2 nm, respectively. Equivalent rms values before and after laser ablation indicate that the laser ablation with 10 and 20 mJ/cm^2 did not contaminate surfaces of PIPAAm-1.4 and -2.9 with ablated debris. Section profiles showed the depth to be 15.5 ± 7.2 nm, indicating the thickness of the grafted PIPAAm layer for PIPAAm-1.4. Likewise, the averaged thickness of PIPAAm grafted layers for PIPAAm-2.9 was 29.3 ± 8.4 nm. Considering the amount and density of the grafted polymer on PIPAAm-1.4 and -2.9, thicknesses of the grafted polymer layers are reasonable.

Cell Adhesion and Detachment Changes on PIPAAm-Grafted Surfaces. Immunofluorescent staining against adsorbed FN was carried out on the surfaces of the PIPAAm-1.4, PIPAAm-2.9, and PIPAAm gel grafted (50 μm thick) glass coverslips (abbreviated as PIPAAm-

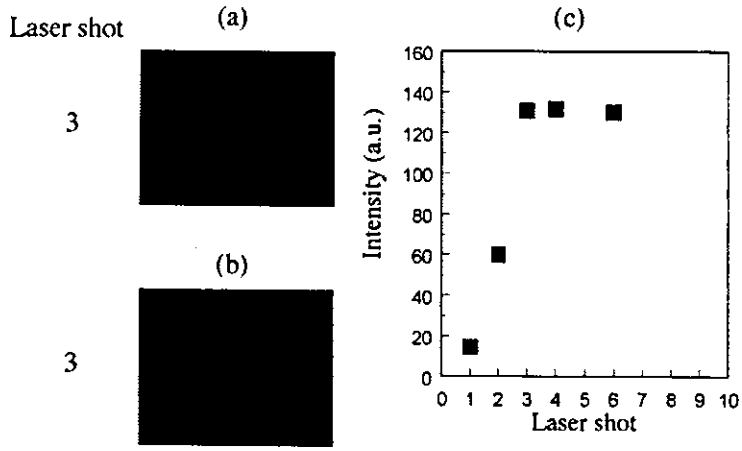

Figure 3. Fluorescence images of the squares on PIPAAm-2.9 surfaces stained by DiIC18 after the UV laser ablation at 10 mJ/cm² (a) and at 20 mJ/cm² (b) for three times. Fluorescence intensity of the domain as a function of the number of UV excimer laser shots at 20 mJ/cm² (c).

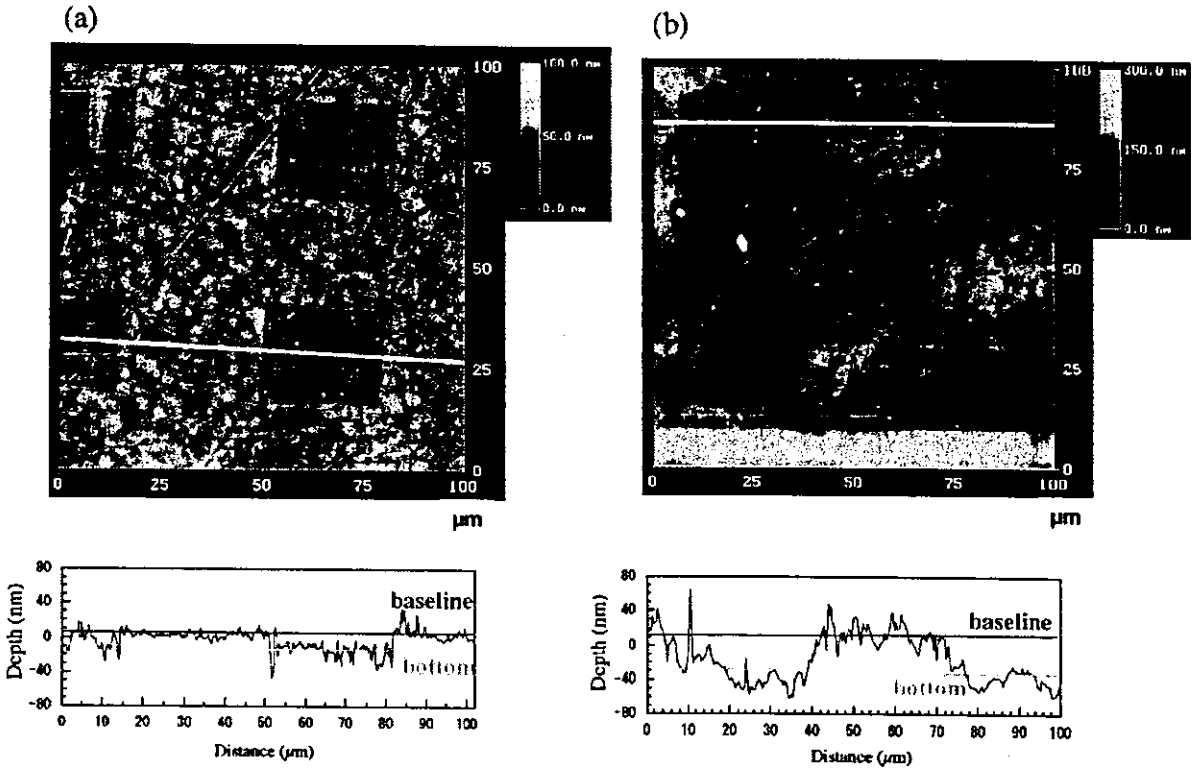

Figure 4. Tapping mode AFM observation for the laser-ablated domains on PIPAAm-1.4 (a) and PIPAAm-2.9 surfaces (b). The laser fluence and the number of irradiations were 10 mJ/cm² and 6 for PIPAAm-1.4 (a) and 20 mJ/cm² and 3 for PIPAAm-2.9 (b). The baseline and the bottom were averages of the text data from the section profiles (see Experimental Section). The scan size was 100 μm × 100 μm.

50). Fluorescence images revealed that FN adsorbed on the surfaces of PIPAAm-1.4. This is in good agreement with a previous report[16] that PIPAAm-modified surfaces with almost the same graft amount showed homogeneous FN adsorption at 37 °C. However, such FN adsorption was not observed on hydrophilic PIPAAm-grafted surfaces at 20 °C.[16] On the other hand, the immunofluorescent images for PIPAAm-2.9 and -50 were not as apparent as that for PIPAAm-1.4, meaning that adsorption of FN for PIPAAm-2.9 and -50 surfaces is negligible. Adsorbed FN for PIPAAm-1.4 and TCPS surfaces was estimated to be approximately 150 and 350 ng/cm², respectively. The amount of the adsorbed FN should be reasonable for ECs to adhere on the PIPAAm-1.4 surfaces,[17] while the estimated value for TCPS is comparable to that of the previous report.[18]

(16) Yamato, M.; Konno, C.; Kushida, A.; Hirose, M.; Utsumi, M.; Kikuchi, A.; Okano, T. *Biomaterials* **2000**, *21*, 981–986.

(17) Iuliano, D. J.; Saavedra, S. S.; Truskey, G. A. *J. Biomed. Mater. Res.* **1993**, *27*, 1103–1113.

(18) García, A. J.; Vega, M. D.; Boettiger, D. *Mol. Biol. Cell* **1999**, *10*, 785–798.

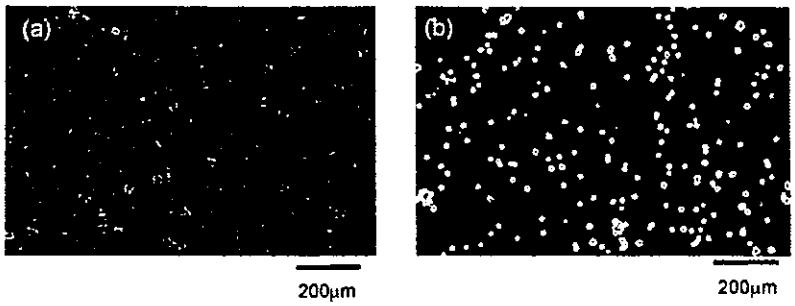

Figure 5. Phase-contrast microphotographs of bovine artery ECs cultured on PIPAAm-1.4 (a) and PIPAAm-2.9 (b) at 37 °C for 1 day.

Table 1. Properties of PIPAAm-1.4, PIPAAm-2.9, and PIPAAm-50[a]

		PIPAAm-1.4	PIPAAm-2.9	PIPAAm-50
density of grafted PIPAAm ($\mu g/cm^2$)		1.4 ± 0.1	2.9 ± 0.1	1080
contact angle (cos θ)	37 °C	0.20	0.35	0.65 (40 °C)
	20 °C	0.42	0.50	0.98 (10 °C)
thickness of the grafted PIPAAm (nm)		15.5 ± 7.2	29.3 ± 8.4	5000
cell attachment/detachment properties	37 °C	yes	no adhesion	no adhesion
	20 °C	yes		
amount of adsorbed FN (ng/cm^2)	37 °C	150 ± 50	UD	UD
	20 °C	UD	UD	UD

[a] UD: Undetectable. Glass coverslips were used as the base substrate of PIPAAm-50. Density and thickness of the grafted PIPAAm were measured in the dry state.

Cell attachment/detachment responses on PIPAAm-grafted surfaces are the key factor for noninvasive recovery of cell sheets for further applications of tissue and organ reconstruction. Here we examined cellular responses to these PIPAAm-grafted surfaces in terms of cell adhesion and detachment with temperature. ECs adhered and spread on the PIPAAm-1.4 dishes (Figure 5a), whereas those on PIPAAm-2.9 did not (Figure 5b). The latter tendency was also observed for PIPAAm-50 (data not shown). Adhered and proliferated cells on PIPAAm-1.4 surfaces were detached from the surfaces by reducing temperature below the PIPAAm's transition temperature in single cells and/or monolayer cell sheets depending on cell density on the surfaces. This phenomenon was consistent with a previous report.[8]

The properties of PIPAAm-1.4, -2.9, and -50 are summarized in Table 1. Taking the water contact angle of the PIPAAm-grafted surfaces at 37 °C into account, these results support that the PIPAAm-50 surfaces are likely to be the most hydrophilic among the three surfaces, although these surfaces exhibit hydrophilic/hydrophobic alterations by temperature. The hydrophobic/hydrophilic properties are influenced by the amount and thickness of the grafted PIPAAm. There should be an optimum content of grafted PIPAAm to exhibit cell adhesion and detachment regulation.

Discussion

In the present study, we utilized the UV laser ablation technique, TOF-SIMS, and AFM methods to estimate the thickness of the PIPAAm-grafted layer on TCPS to correlate with cell adhesion/detachment behavior. Chan et al.[19] showed that a laser fluence of the UV excimer laser above ca. 50 mJ/cm^2 influenced the contact angles of resulting polystyrene film surfaces due to chemical property changes and the formation of debris. The laser fluence at 10 and 20 mJ/cm^2 was used for the ablation of PIPAAm-grafted surfaces to attain exposure of TCPS, avoiding the debris formation and any chemical property changes of the resulting surfaces. This was confirmed with fluorescent images and TOF-SIMS results. Surface topology before and after the laser ablation was not altered, also indicating much less contamination with the debris.

In our previous reports, the configuration and resulting dynamic motion of the grafted PIPAAm chains significantly influenced surface wettability in response to temperature changes.[1,2] We prepared one-side fixed PIPAAm hydrogels with glass coverslips and investigated the temperature-dependent swelling/deswelling changes. Compared with nonfixed hydrogels of 500-μm-thick gels, swelling was significantly restricted for one-side fixed gels (unpublished data). We then compared the swelling behavior of one-side fixed gels having different gel thicknesses. The swelling ratio for the thinner gels was less than half of that for the fixed gels with double thickness. These results imply that the molecular motion of the fixed and cross-linked chains is dramatically restricted. Such influences may be significant in the vicinity of matrix surfaces. These considerations are extended to discuss the differences in surface property alterations with PIPAAm-grafted surfaces having different graft amounts. Figure 6 illustrates a schematic drawing of the differences in molecular motion of grafted PIPAAm chains on two types of PIPAAm-grafted surfaces at 20 and 37 °C. An arrow with a gradient of black color illustrates the degree of the molecular motion. The darker polymer chains represent more restricted molecular motion, while brighter chains are more mobile. In the case of the ultrathin PIPAAm gel layers on TCPS, hydrophobic interaction at TCPS interfaces (indicated as a black region between TCPS and PIPAAm chains) is also likely to promote aggregation and enhanced dehydration of the covalently bound PIPAAm chains. The hydrophobic and immobile TCPS interfaces restrict molecular motion of the PIPAAm grafted chains (darker networks in Figure 6). Such restriction of chain mobility should be extended to the outermost regions of PIPAAm chains for PIPAAm-1.4. Thus, PIPAAm-1.4 was relatively more hydrophobic

(19) Chan, C. M.; Ko, T. M.; Hiraoka, H. *Surf. Sci. Rep.* **1996**, *24*, 1–54.

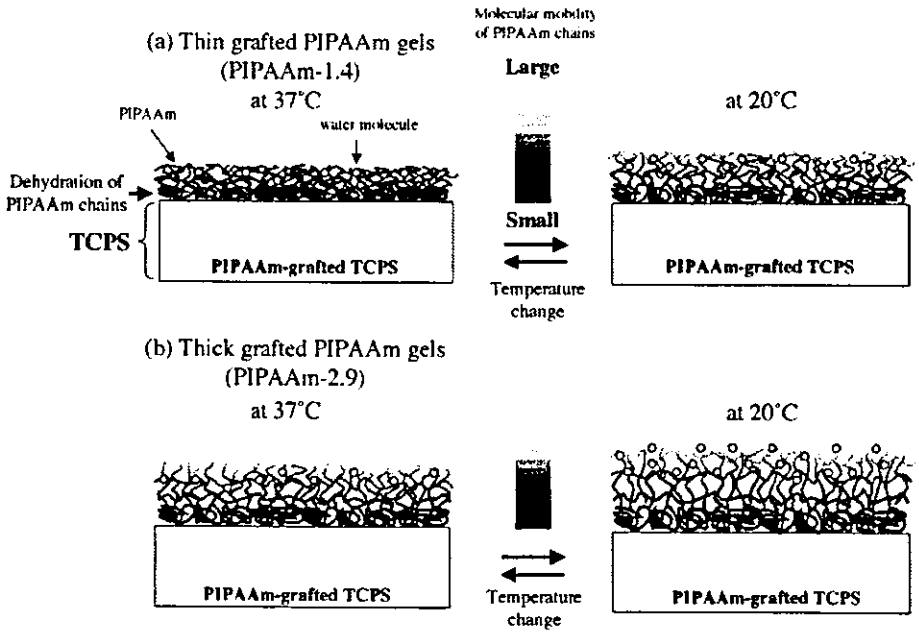

Figure 6. Schematic drawings of the influence of molecular motion of grafted PIPAAm chains on hydration of the polymer chains, when the grafted PPAAm gels are thin (a) and thick (b) at 20 °C (left side) and 37 °C (right side), respectively. Hydrophobic TCPS interfaces promoting aggregation and dehydration were represented as a black region in TCPS. Molecular motion of the grafted polymer chains becomes larger according to the distance away from TCPS interfaces.

than PIPAAm-2.9. For the thicker polymer grafted gel of PIPPAm-2.9, more polymer chains at the outermost regions are hydrated than those on PIPAAm-1.4-grafted surfaces (Figure 6b). In other words, as illustrated schematically in Figure 6b, more hydration for PIPAAm-2.9 surfaces should be occurring than for PIPAAm-1.4. Such changes greatly influence the contact angle changes and cell adhesion/detachment behavior. The observed cell adherent and nonadherent surface characteristic changes occur in only 15–20-nm differences for the examined surfaces. Membranes prepared by the solvent-cast method usually have thicknesses in the range of several micrometers. Such thicker PIPAAm-coated surfaces showed nonfouling characteristics to cells without addition of cell adhesion proteins such as collagen[20] and gelatin components.[21] Such a non-cell-adherent property is also seen for PIPAAm-50 (Table 1). Covalent bonds of the PIPAAm-50 gels on the solid glass coverslips resulted in the restricted molecular motion of the grafted polymer chains, inducing suppressed gel swelling. However, as was seen in Table 1, the outermost gel surfaces showed more polar characteristics than nanometer-thick PIPAAm gel grafted surfaces in terms of the surface wettability even at 37 °C. Electron beam irradiation polymerization is extremely essential for design of the nanometer-thick interfaces to regulate grafted PIPAAm thickness and the following cell adhesion/detachment control by temperature.

(20) Takezawa, T.; Mori, Y.; Yoshizato, K. *Bio/Technology (NY)*, **1990**, *8* (9), 854–856.
(21) Morikawa, N.; Matsuda, T. *J. Biomater. Sci., Polym. Ed.* **2002**, *13*, 167–184.

Conclusions

In the present study, we demonstrate that thickness and the amount of grafted PIPAAm layers have significant influence on surface properties in terms of thermoresponsive cell adhesion and detachment and approximately 20-nm thickness is the key factor for the PIPAAm-grafted surface to achieve adhesive cell adhesion and detachment with temperature. Progressive dehydration of PIPAAm chains existing at the vicinity of hydrophobic TCPS may be important to show cell adhesion character at 37 °C. By contrast, the graft polymer at the outermost interfaces of PIPAAm-2.9 should have more polar characteristics even at 37 °C than PIPAAm-1.4, which causes cells not to adhere on it.

Acknowledgment. This work was partly supported by a Grant-in-Aid for Scientific Research (Grant No. 13308055), the Japan Society for Promotion of Science (JSPS), and carried out under the Center of Excellence (COE) Program for 21st Century, "The Center for Tissue Engineering and Regenerative Medicine", the Ministry of Education, Culture, Sports, Science and Technology (MEXT), Japan.

LA036139F

厚生労働省科学研究費補助金　ヒトゲノム・再生医療等研究事業

組織工学による血管増生心筋組織の構築並びにその移植による血管床の再生

平成１５～１６年　総合研究報告所 VOL.1

発行者：国立循環器病センター研究所心臓生理部　部長　盛英三

〒565-8565　大阪府吹田市藤白台５－７－１

TEL:06-6833-5012（内線 2530）、FAX:06-6835-5416

発行日：平成１７年３月３１日

印刷所：株式会社ジップ

厚生労働省科学研究費補助金

ヒトゲノム・再生医療等研究事業

組織工学による血管増生心筋組織の構築ならびにその移植による冠血管床の再生

総合研究報告書 VOL.2

主任研究者　盛　英三

平成１７年３月

厚生労働省科学研究費補助金

ヒトゲノム・再生医療等研究事業

組織工学による血管増生心筋組織の構築ならびにその移植による冠血管床の再生

総合研究報告書 VOL.2

主任研究者　盛　英三

平成１７年３月

目次

FEBS Letters 565 (2004) 6–10 FEBS 28299

Human limbal epithelium contains side population cells expressing the ATP-binding cassette transporter ABCG2

Katsuhiko Watanabe[a], Kohji Nishida[a,*], Masayuki Yamato[b], Terumasa Umemoto[b], Taizo Sumide[a], Kazuaki Yamamoto[a], Naoyuki Maeda[a], Hitoshi Watanabe[a], Teruo Okano[b], Yasuo Tano[a]

[a]*Department of Ophthalmology, Osaka University Medical School, Room E7, Yamadaoka 2-2, Suita, Osaka 565-0871, Japan*
[b]*Institute of Advanced Biomedical Engineering and Science, Tokyo Women's Medical University, 8-1 Kawada-cho, Shinjuku-ku, Tokyo 162-8666, Japan*

Received 9 January 2004; revised 9 March 2004; accepted 9 March 2004

First published online 7 April 2004

Edited by Veli-Pekka Lehto

Abstract Many types of organ-specific stem cells have been recently shown to exhibit a side population (SP) phenotype based on their ability to efflux Hoechst 33342 dye. Because stem cells from corneal epithelium reside in the basal layer of the limbal epithelium, the purpose of this study was to examine whether the limbal epithelium contains SP cells. The ATP-binding cassette transporter Bcrp1/ABCG2 is reported to contribute to the SP phenotype in cells from several diverse sources. Here we show data from fluorescence-activated cell sorting and real-time quantitative RT-PCR analysis showing that harvested limbal epithelial cells contain SP cells expressing ABCG2. Immunofluorescence revealed that a portion of limbal epithelial basal cells expressed ABCG2. Data indicate that ABCG2 positive limbal epithelial cells are putative corneal epithelial stem cells.

Keywords: Corneal epithelium; Limbal epithelium; Stem cell; Side population; ABCG2

1. Introduction

The cornea – the transparent outer anterior tissue layer of the eye – provides the eye with protection and refractive properties essential for vision. These functions depend, in part, on the corneal epithelium, a highly specialized cell layer comprising both basal and stratified squamous cells. Corneal epithelial stem cells reside in the basal layer of the limbus [1,2], the transitional zone between the cornea and the more peripheral bulbar conjunctiva. These cells allow the renewal of the corneal epithelium by generating transient amplifying cells that migrate, proliferate and differentiate to replace lost corneal epithelial cells [3–5]. However, because of the absence of the definite biological markers, unequivocal corneal epithelial stem cell identification remains elusive.

In 1996, Goodell et al. [6] demonstrated that mouse hematopoietic stem cells with long-term multi-lineage reconstituting ability can be isolated as side population (SP) cells based on their ability to efflux the Hoechst 33342 dye. Using dual wavelength flow cytometric analysis, SP cells were identified as a distinct population with low Hoechst 33342 blue/red fluorescence representing approximately 0.1% of total bone marrow cells [6]. SP cells have also been identified in hematopoietic compartments in a number of animals [7–10]. In addition, SP cells have been isolated from various types of adult tissue where they demonstrate stem cell activity [6,10–16]. These findings suggest that the SP phenotype represents a common feature of stem cells.

Recently, Zhou et al. [13,17] reported that the ATP-binding cassette transporter Bcrp1/ABCG2 is a molecular determinant of the SP phenotype. A number of other studies in a wide variety of organs have also indicated that the SP phenotype is largely determined by the expression of Bcrp1/ABCG2 [13,15,18–20]. More recently, Mogi et al. [21] have shown by targeted gene ablation studies in mice that serine/threonine kinase Akt signaling modulates the SP phenotype by regulating the expression of Bcrp1/ABCG2.

At present, it remains unclear if corneal epithelial stem cells might exhibit the SP phenotype. We report our recent studies on human limbal epithelium, providing evidence that these cells contain SP cell subsets expressing ABCG2, implicating possible relationships between these SP cells and limbal stem cells.

2. Materials and methods

2.1. Cell preparation

Human corneoscleral rims from USA eye bank eyes were used. Limbal tissues were obtained by using scissors, and 8.0-mm diameter central portions of corneas were obtained by trephination. Limbal tissues and central corneas were incubated separately at 37 °C in Dulbecco's modified Eagle's medium (DMEM; Nikken Biomedical Laboratory, Kyoto, Japan) containing 2.4 units/ml dispase (Invitrogen, Carlsbad, CA) for 1 h. Epithelial cells were separated under a dissecting microscope and treated with 0.25% trypsin-1 mM EDTA solution (Invitrogen) for 15 min at 37 °C to achieve each single cell suspensions from the limbal epithelium and the corneal epithelium. Enzymatic activity was then stopped by adding an equal volume of DMEM containing 10% fetal calf serum (FCS; Morgate Biotech, Qld., Australia).

2.2. Hoechst 33342 dye exclusion assay

Separate populations of epithelial cells from the limbus and from the cornea were resuspended at 1.0×10^6 cells/ml in incubation medium

* Corresponding author. Fax: +81-6-6879-3458.
E-mail address: knishida@ophthal.med.osaka-u.ac.jp (K. Nishida).

0014-5793/$22.00
doi:10.1016/j.febslet.2004.03.064